The Meteoritical Society

Meteoritics & Planetary Science 43, Nr 6, 1085–1095 (2008)
Abstract available online at http://meteoritics.org

Finite difference time domain simulation of radar wave propagation through comet nuclei dielectric models

Ruth A. CARLEY[1, 2*] and Essam HEGGY[3]

[1]The University of Cambridge, Fracture Group, Cavendish Laboratory, J. J. Thompson Avenue, Cambridge CB3 0HE, UK
[2]Present address: The School of Geosciences, Grant Institute of Earth Science, University of Edinburgh, West Mains Road, Edinburgh EH9 3JW, UK
[3]Lunar and Planetary Institute, 3600 Bay Area Boulevard, Houston, Texas 77058, USA
[*]Corresponding author. E-mail: r.a.carley@cantab.net

(Received 16 February 2007; revision accepted 31 October 2007)

Abstract–The 90 MHz radar-wave experiment, Comet Nucleus Sounding Experiment by Radiowave Transmission (CONSERT), on board the Rosetta mission (ESA, 2004) is expected to probe the nucleus of the comet 67P/Churyumov-Gerasimenko (67P/C-G) to reveal information on its physical properties, chemical composition, and internal structure. This investigation assesses the potential to recognize lithological structure in the comet nucleus with a radar experiment such as CONSERT. Radar simulations at 90 MHz were performed with a finite difference time domain (FDTD) method. The amplitude and losses of the transmitted and reflected electric field components of an incident radar pulse were evaluated as a function of time. Seven different dielectric models of sections of a hypothetical comet nucleus were used, representative of existing theories of comet nuclei. Values of dielectric constant assigned to these models are based on mixing laws for a porous mixture of ice and meteoritic dust, employing laboratory measured values of relative permittivity for mainly chondritic meteorites. Our results confirm that structural differences such as layers or inclusions are discernable from transmitted and reflected radar signals at 90 MHz, the central frequency of the CONSERT instrument. Such simulations help to constrain the ambiguities that might exist in future radar data associated with the nature of the comet nuclei, whether conglomerate or layered in nature.

INTRODUCTION

The nature of the comet nucleus has been the subject of debate and interest for decades. New observations from the Rosetta mission are intended to help resolve some of the fundamental questions associated with the origin, composition, and evolution of comets, by studying comet 67P/Churyumov Gerasimenko (67P/C-G). The mechanism of formation of the comet nucleus, and its resulting internal structure is dependent on the initial conditions in the region of comet formation. As primitive building blocks of the solar system, an understanding of the composition, structure and formation of cometary nuclei will provide crucial knowledge on the chemical and physical conditions in the early planetary nebula at the time of planet formation.

The European Space Agency's Rosetta mission (2004–2014) will rendezvous with comet 67P/C-G, and orbit its nucleus performing remote sensing investigations of the comet surface and interior. The Rosetta mission contains among other experiments, the Comet Nucleus Sounding Experiment by Radiowave Transmission (CONSERT), which will probe the nucleus of comet 67P/C-G using 90 MHz radio waves to reveal information on its physical properties, chemical composition, and internal structure (Kofman et al. 1998).

Comet 67P/C-G is a dusty, short period (<200 yr), Jupiter family comet thought to originate from the trans-Neptunian Edgeworth-Kuiper belt at 35–50 AU and beyond (Farinella and Davis 1996). It is an approximate ellipsoid (observed from the Hubble Space Telescope) (Lamy et al. 1998), with recent estimates for the semi-major and semi-minor axes giving between 2.45 and 3.20 km, and 1.40 and 1.85 km, respectively (Davidsson and Gutiérrez 2005).

The CONSERT instrument consists of a lander deployed to the surface of the comet, transmitting 90 MHz radar waves through the comet nucleus to the orbiting spacecraft (Barbin et al. 1999). Radar waves passing through the comet nucleus will be subject to scattering and reflection from internal structures, and attenuation and velocity changes determined by the complex relative permittivity (also referred to as the dielectric constant) of the nucleus.

The amplitude of the radar signal transmitted through the comet to the orbiting spacecraft will be measured as a function of time for different propagation paths through the comet, achieved over several orbits. Radar waves reflected from internal structures received by the lander will also be recorded. Analysis of the amplitude and attenuation of these reflected and transmitted signals will be used to place constraints on the dielectric description of the comet. This will be used to asses the structure and composition of the comet nucleus. A computed tomography of the internal structure of the comet nucleus can also be built up from inversion of the attenuated transmitted radar signal for each propagation path (Hérique et al. 1999).

The main aims of the CONSERT experiment as summarized by Kofman et al. (1998) are (1) the derivation of the average dielectric constant of the comet nucleus to infer its composition, (2) the detection of the presence of large (meter-sized) structures and stratifications, and (3) the detection of smaller scale irregularities in the comet.

The investigation described in this paper assesses the potential for achieving the second aim of the CONSERT experiment—to infer the structure of the comet nucleus from the propagation (transmission and reflection) of radar waves through the nucleus. This was carried out by simulating radar wave propagation through different dielectric models of comet nuclei to examine the variations in the radar returns due to different structures and compositions. Previous radar simulations for model comet nuclei (Barriot et al. 1999; Benna et al. 2002) have used geometrical optics to study ray propagation, tracing rays through comet models with small ($<<\lambda$) inclusions of dust in ice, applying Snell's law at interfaces. While such an approach was necessary to provide a first insight into radar propagation through relatively homogenous cometary models, an update was needed to simulate the radar returns from more complex and relevant cometary models.

In this investigation we used the finite difference time domain (FDTD) technique to solve the Maxwell equations to obtain the magnitude of the reflected and transmitted electric field at each point inside the dielectric profile. Few electromagnetic methods can be adapted to properly describe wave propagation in heterogeneous materials exhibiting a variety of dielectric and geometric structural elements, as is the case for cometary nuclei. The major advantage of the FDTD algorithm is its flexibility in terms of using a wide variety of material dielectric properties, geometries, and frequencies (Kunz and Luebbers 1993). The technique is briefly described later on.

Simple three-dimensional dielectric models of sections of comet nuclei used in this investigation are intended to be representative of the current theories and state of knowledge for comet nuclei structure. These structures are briefly discussed in the next section, followed by a description of the electromagnetic characterization of seven sections of model comet nuclei with features such as layers, or inclusions of different size ($>\lambda \sim 3$ m), volume percent, and composition. The values of dielectric constant for the cometary material are calculated from mixing laws for porous ice and dust, using laboratory measured values of relative permittivity for meteoritic dust. The reflected and transmitted radar signals resulting from an incident pulse at 90 MHz for each of these models produced from the FDTD simulation are described in the Results section and discussed to assess the effect of comet structure and composition on radar propagation.

THEORETICAL MODELS OF COMET NUCLEI

Comet nuclei are irregular bodies thought to be composed of ice and dust, but their internal structure is unknown. Several models, briefly summarized below, have been proposed for the comet nucleus (Weissman et al. 2004).

One of the first models proposed for the comet nucleus was the "homogenous icy conglomerate" ("dirty snowball") (Whipple 1950) consisting of water ice and other volatiles such as carbon dioxide, combined in a conglomerate with meteoritic material. This model could account for the low bulk density of comets and explained many other aspects of cometary behavior such as their non-gravitational motion resulting from sublimating ices on the surface of a rotating nucleus. This model assumed a single body and did not comment on the underlying structure of the nucleus.

Direct observation of comets with radar (Goldstein et al. 1984) and from exploration missions such as Giotto and Vega (1986, comet Halley), showed them to have irregular local topographic features. These observations led to the "fractal aggregate" (Donn 1990), "rubble pile" (Weissman 1986), and "icy glue" (Gombosi 1986) models proposed for comet nuclei, incorporating aggregates of smaller icy planetesimals within the nucleus. In the "fractal aggregate" model, the nucleus is proposed to consist of grains of ice and dust randomly accumulated in aggregates of different sizes (from μm to km), while the "rubble pile" model consists of loosely bound smaller fragments proposed to be similar in composition to the outer asteroids. In contrast to the loosely bound "fractal aggregate" and "rubble pile" models, the "icy glue" model has the nucleus composed of large (tens of cm to hundreds of m) porous refractory boulders within a background matrix of ice and dust.

Recently there has been much evidence in favor of the "rubble pile" nature of the comet nucleus, particularly from the breakup of comets such as comet Shoemaker-Levy, another Jupiter family comet. Models of this breakup (Scotti and Melosh 1993; Asphaug and Benz 1994) which can account for the observed "string of pearls" of ~20 fragments, require several hundred smaller aggregates to be bound gravitationally, forming a strength-less structure. These fragments may be smaller comets or boulders brought together as a result of collisional processes occurring in the region of formation (Farinella and Davies 1996). Not all "rubble pile" models need to be strength-less as they may evolve into a bonded structure, "cemented" together with an ice-dust mixture.

The most recent model for the comet nucleus predicts a "layered pile" model (Belton et al. 2007). This is based on observations of widespread layering and topographical features on the surface of Jupiter family comets from passing spacecraft (Brownlee et al. 2004). These layers are thought to be several meters to several tens of meters thick, built up over an icy core as a result of low-velocity collisions with other primitive bodies. Thermal activity in comets could also cause stratification of the nucleus due to the successive temperature increase towards the surface, ice vaporization and ice crystallization (Prialnik 2004). Most comet models also include an outer dust layer, formed as the comet approaches the Sun and the icy volatiles sublimate from the surface of the nucleus. The porous dusty mantle left behind is 1–15 m thick with porosity of up to 80% (Prialnik 1998).

In order to evaluate the potential for radar to distinguish between the different structural and lithological elements predicted in these theoretical nuclei, it is necessary to represent the main features of a comet nucleus with dielectric models utilizing electromagnetic characteristics of cometary analog materials.

DIELECTRIC MODELS OF COMET NUCLEI

Electromagnetic Characterization of Cometary Material

The principal ice in comets (~80%) is thought to be amorphous water ice (Rickman 1993) with minor constituents of carbon dioxide, carbon monoxide, and some organic species making up the remaining volatile content. Cometary dust, as observed in comet comae (Langevin et al. 1987) and from Deep Impact (Harker et al. 2005) is a mixture of micrometer-sized grains of crystalline silicates such as pyroxene and olivine, with composition range similar to that encountered in carbonaceous chondrites. Smaller amounts of "light element" dust (carbon, hydrogen, oxygen, and nitrogen) in the form of complex or simple molecules are also expected. The dust content of comets may comprise up to 75% of the mass and 50% of the comet volume (Skyes and Walker 1992). Comets are very porous bodies and have the lowest densities observed in the solar system (Rickman 1993). Non-gravitational effects on the motion and orbit of comet 67P/C-G have been used to place observational constraints on the density and porosity of its nucleus. The bulk density has been estimated with an upper limit of 600 kg m^{-3}, and the porosity as much as 70% (Davidsson and Gutiérrez 2005).

In this investigation, the composition of comets is considered as a porous mixture of ice and meteoritic dust. Values of complex relative permittivity ($\varepsilon_r = \varepsilon_r' - i\varepsilon_r''$), and electrical conductivity (σ, calculated at 90 MHz from ε_r'') were calculated for six representative (though not necessarily definitive) cometary materials (Table 1).

The outer dusty layer of the comet was assigned the highest value of porosity, and hence lowest value of dielectric constant. These values were calculated from Lichteneker's mixing laws (Parkhomenko 1967) with different porosities and ice and meteoritic dust content using a theoretical relative permittivity and conductivity value for pure ice, and an average laboratory measured value for meteoritic dust (Table 2). This average relative permittivity value was for a variety of chondritic meteorites, ground to a fine homogeneous powder (50 μm) and compacted to a density close to that estimated by Davidsson and Gutiérrez (2005). The relative permittivity was measured with an impedance analyzer, as described in Heggy et al. (2007), and the value taken at 90 MHz, the central frequency of the CONSERT experiment. The meteoritic dust particles in the ice are assumed to be non-magnetic (relative magnetic permeability $\mu_r = 1$), devoid of magnetic minerals such as magnetite. In our approach, the dust particles are small enough (1 μm to a few tens of mm, $<<\lambda$) to be incorporated in the bulk material properties rather than being considered as separate inclusions in the ice.

It should be noted that relative permittivity is expected to increase with increasing density (Carley and Heggy 2006) and also to vary with temperature (Heggy et al. 2006b). This could introduce some dielectric variations with depth, resulting from thermal or lithological variation in the comet nucleus not considered in these first-order models. These variations are mainly dominated by changes in density within the nucleus which are, thus far, uncharacterized due to lack of observations and a high degree of ambiguity in such modeling. Hence, for the purpose of modeling discrete sections of the comet nuclei only, we will not consider the effect of density or temperature on dielectric properties as the variation within our simulation space (~50 m for each section) will be minor. Under such a case, the mixing laws for the compositional dependence provide sufficiently accurate values of relative permittivity.

Measurement of relative permittivity values for comet analog materials taking account of conditions of temperature, density, and ice contaminated with meteoritic dust are described by Heggy et al. (2006a). In-situ measurements of the surface of the comet, carried out by the lander deployed by Rosetta, will provide a ground truth for the modeling of the surface dielectric constant that will be useful in the interpretation of the radar data.

Comet Section Models

The seven comet nuclei dielectric models (Table 3) used for these simulations are intended to be representative of the main features of the theoretical models described previously, but we also recognize that alternative structures exist. These models allow the examination of the effects of different structural and textural features, such as layers and agglomerations of different size and dielectric constant, on the resulting simulated transmitted and reflected radar signals. The homogenous comet nuclei models act as a

Table 1. Electromagnetic characterization of cometary materials for comet models.

Material	Porosity	Ice	Meteoritic dust	ε_r'	ε_r''	σ (mSiemens m^{-1})
Dust layer	70%	–	30%	1.62	0.0009	0.0045
Porous icy matrix	60%	30%	10%	1.63	0.0003	0.0015
Icy matrix	40%	40%	20%	2.14	0.0006	0.003
Porous “dirty ice”	20%	40%	40%	2.95	0.0012	0.006
Porous rocks	20%	–	80%	3.62	0.0024	0.012
“Dirty ice”	–	50%	50%	3.87	0.0012	0.0075

Table 2. Relative permittivity and electrical conductivity values used in mixing laws.

	ε_r'	ε_r''	σ (mSiemens m^{-1})
Pure ice[1]	3.00	0.00	0.00
Meteoritic dust[2]	5.00	0.003	0.015
Free space	1.00	0.00	0.00

[1]Theoretical value, for example (Petrenko 1999) with no distinction made for amorphous or crystalline ice.
[2]Average value for LL5, L5 and H5 chondrites.

reference model to examine these effects, and agglomerations are considered as inclusions in a background matrix of contrasting relative permittivity rather than with voids.

Computational memory constraints on the size of the simulation environment limit the volume of the model geometry. As a result, these models are not expected to model the whole of the comet interior at once, but represent sections of comet nuclei. An insight into the simulated radar response for the full size comet nucleus can be obtained by summing the radar responses from each comet section with a time delay to form the equivalent transmission and reflection profile for propagation across the whole geometry.

Each section model was produced in a three-dimensional model geometry space (Fig. 1), 100 m × 100 m × 50 m, with a 5 m thick top porous dust layer. A model two times wider than its thickness cuts down the effect of clutter on the received signal from simulated waves reflected from the edges of the model geometry. At the base we introduced a layer of perfect electrical conductor (PEC) to act as a reflective layer to identify the end of the geometry in the reflected radar signal.

Comet models with structure from agglomerations were modeled with large (>λ) uniform spherical inclusions of varying size, volume percent, and dielectric constant, positioned randomly in a background icy matrix. The smaller icy inclusions in the background icy matrix offer an approximate model of an “icy glue” nucleus, and the larger volume percent of inclusions represent the “fractal aggregate” nucleus (however, this model is likely to show more variation in aggregate size and higher porosity not considered in this study). The increased dielectric contrast between the background matrix and the “rocky” inclusions are intended to represent the “rubble pile” theory of the comet nucleus.

The effect of layers was studied with a simple three layer model with parallel, homogeneous layers 16 m thick, with increasing dust content and relative permittivity with depth. The model geometries for the homogeneous models, layered model, and models with inclusions can be seen in the time sequence slides of Fig. 2. These dielectric models are meshed into a profile of cubic cells in the simulation space. Each cell describes the real relative permittivity and conductivity of the occupied volume and provides a finite step size for the FDTD simulation.

FDTD SIMULATION OF THE RADAR SIGNAL

The FDTD method for the simulation of the propagation of electromagnetic waves through a dielectric (and magnetic) material is a transient marching in time approach, in which time and space are divided into small discrete steps (Yee 1966). We set the elementary cell dimension in the simulation space at 0.25 m to give the typical value of 10 cells per wavelength in the material with the highest relative permittivity. This ensures sufficient temporal accuracy and respects the algorithm stability conditions. The total simulation space consisted of the dielectric model surrounded by 10 cells of free space and bounded by an absorbent layer. This layer used the perfect matching layers (PML) algorithm with six layers to act as an electromagnetic absorbent around the simulation space to reduce the simulation noise from boundary reflections.

To simulate the electromagnetic wave emitted from the Rosetta lander, a Gaussian pulse waveform 15 ns long with a central frequency of 90 MHz was applied to a model linear antenna (X-axis aligned) in the center of the surface of the model geometry (Fig. 1). The FDTD method then calculates the three-dimensional components of the electric and magnetic fields at each time step after the radar pulse illumination to simulate the radar wave propagation across the meshed dielectric profile.

The magnitude of the total (scattered and incident) electric field in the two cross polarizations, *Ex* and *Ey*, of the simulated wave pulse was recorded at the top and bottom of the dielectric model to observe the reflected and transmitted waveforms respectively over a time period of 1000 ns. The normalized time varying electric field magnitude for each simulation was also recorded as a sequence of slides to show the propagation, and losses in decibels (dB) of the initial incident waveform through the center of the dielectric model in the *ZY* plane. These slides are useful to identify the origin of features in the reflected and transmitted signals and the timing of the onset of clutter from the corner reflections. Time

Table 3. Description of the seven representative dielectric models used in the radar simulations.

Model name	Material description[1]
Homogeneous	Icy matrix
Homogenous porous	Porous icy matrix
3 layers	Icy matrix over porous "dirty ice" over "dirty ice"
Spherical inclusions[2] (20%, 5 m radius)	Porous "dirty ice" inclusions in icy matrix
Spherical inclusions (20%, 15 m radius)	Porous "dirty ice" inclusions in icy matrix
Spherical inclusions (40%, 5 m radius)	Porous "dirty ice" inclusions in icy matrix
Spherical inclusions, rocky (40%, 5 m radius)	Porous rocky inclusions in icy matrix

[1]See Table 1 for electromagnetic characterization of each material.
[2]Inclusion percentages are by volume.

sequences for the homogenous model, layered model and model with inclusions are shown in Fig. 2.

RESULTS

Figures 3–9 show the reflected and transmitted radar amplitudes in micro volts per meter (μVm^{-1}), (Figs. 3–9, parts a and c, respectively) and the reflected and transmitted losses in dB (parts b–d, respectively), normalized to the maximum value of electric field (corresponding to the surface reflection), as a function of time for the *Ex* component of the electric field for simulated 90 MHz radar propagation. Figures 3 and 4 are for propagation through the homogeneous dielectric models and Fig. 5 for the layered model. Figures 6–9 are for radar propagation through the dielectric models with 20 volume percent 5 m (Fig. 6) and 15 m (Fig. 7) radius inclusions, and 40 volume percent 5 m radius inclusions with porous (Fig. 8) and rocky (Fig. 9) composition.

The reflected radar signals (Figs. 3–9a) contain the emitted radar pulse in its first 150 ns as this signal was recorded at the top of the model geometry. Reflections from the dust layer (possibly multiple) cannot be distinguished from the emitted pulse. The reflection from the PEC layer at the base of the modeling space is received from about 600 ns onwards, with amplitudes of around 500 μVm^{-1} for the homogeneous and layered models (Figs. 3a, 4a, and 5a), and up to 1000 μVm^{-1} for the models with inclusions. Reflections from features such as layers or inclusions, and also from the corners, arrive earlier than the base reflection.

For these model sections, the first transmitted signals are received after about 250 ns with amplitudes of around 2000 μVm^{-1} for the homogeneous models (Figs. 3c and 4c), layered model (Fig. 5c) and model with 15 meter radius inclusions (Fig. 7c), and at around 1000 μVm^{-1} for the models with 5 m radius inclusions. The transmission amplitudes are larger because they represent one-way propagation only. Reflections from the top and bottom corners of the model geometry are received later in transmission, from about 550 ns as observed in the homogeneous models (Figs. 3c and 4c). Arrival times for the reflected and transmitted signals can be converted into distance traveled knowing the dielectric properties of the models, which determine the propagation velocity of the electromagnetic wave in each material.

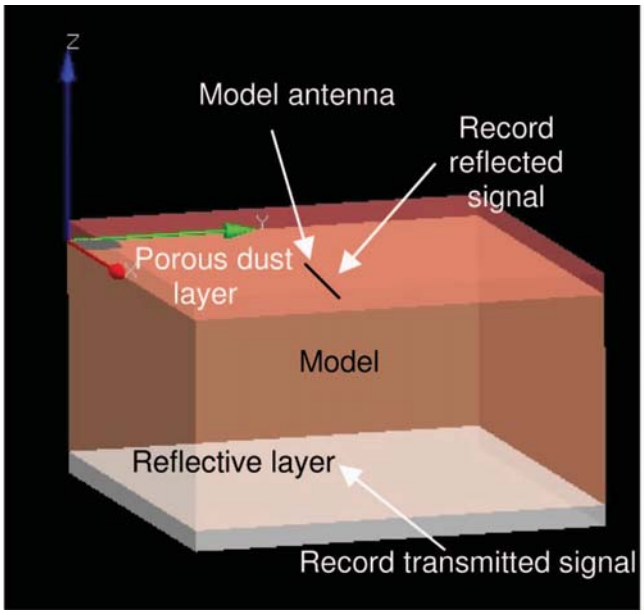

Fig. 1. Three-dimensional simulation space showing 100 m × 100 m × 50 m dielectric model with 5 m top porous dust layer and perfect electrical conductor as a reflective base layer. Locations of the linear antenna (thin wire) and sites of recorded signals are shown.

The normalized losses for the reflected signals (Figs. 3–9b) show an initial exponential increase as the emitted signal decays, before reflections from inclusions or layers arrive. The arrival of radar reflections then produce peaks in the normalized loss curves. The exponential attenuation of the transmitted waveform can also be seen in the normalized losses of the transmitted signals after the first transmission for the homogeneous models (Figs. 3d and 4d), but is overcome by other reflections in the models with layers or inclusions. The modulation of the signal in the normalized loss curves represents the time variation in the emitted signal, and simulation noises.

It must be noted that the amplitude of the radar signal will decrease with distance traveled (and hence time) from the surface transmitter due to geometric spreading of the waveform, as well as dielectric attenuation. As the radar transmitter and receiver in the CONSERT instrument are separated by nearly twice the comet diameter, the propagating radar waves can be considered as plane waves and are hence

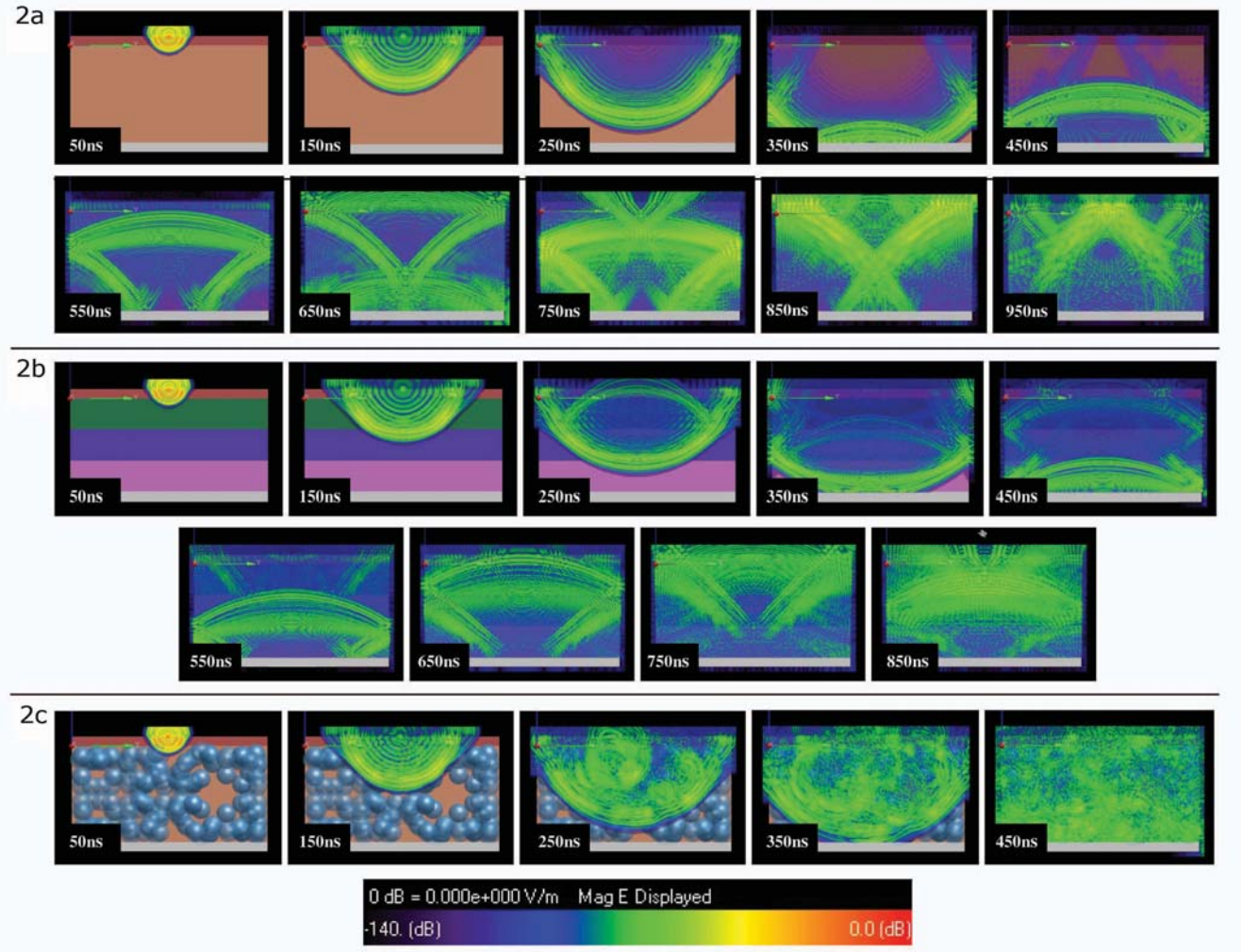

Fig. 2. Time sequence slides in 100 ns separation of the simulated radar wave propagation as recorded in the center of the model in the *ZY* plane showing the normalized magnitude of the electric field vector in dB for a homogeneous model (2a), layered model (2b), and model with inclusions (20 volume percent, 5 m radius) (2c).

less likely to suffer from geometric spreading. Consequently, the absolute magnitude of the normalized losses and reflected and transmitted radar waves in this simulation will not be totally comparable to the magnitudes of signals in the final processed radar data considered by CONSERT. However, the properties of the transmitted and reflected signals and their loss curves resulting from the effects of internal structure will be directly comparable to properties in the CONSERT radar returns.

The discussion of these results mainly considers the *Ex* component of the electric field as this is the principally emitted polarization of the simulation (some *Ey* is also emitted as the wire antenna is in contact with the dielectric surface dust). Reflections from boundaries at layers or inclusions cause a change in polarization, allowing the magnitude of the *Ey* signals to be used as an extra source of information on the internal structure. The *Ey* component amplitudes show similar features as *Ex* but with much smaller magnitudes (~5 μVm^{-1}) in the case of the homogeneous and layered models. The arrival time of the main transmitted *Ey* signal is slightly behind the transmitted *Ex* signal as more depolarization of the emitted *Ex* signal occurs with time due to multiple reflections. As the *Ey* signals are small, the normalized losses before reflections from the corners occur are higher (particularly in transmission).

DISCUSSION

Discussion of the results of the radar simulations for these dielectric models are considered in terms of the effects of structure (Figs. 3–6), and the effect of inclusions of different size and composition (Figs. 6–9) on the simulated radar propagation.

The Effect of Structure

Propagation through a dielectric material causes broadening of the reflected and transmitted waveforms due to the slowing of the radar wave in the material. This signal

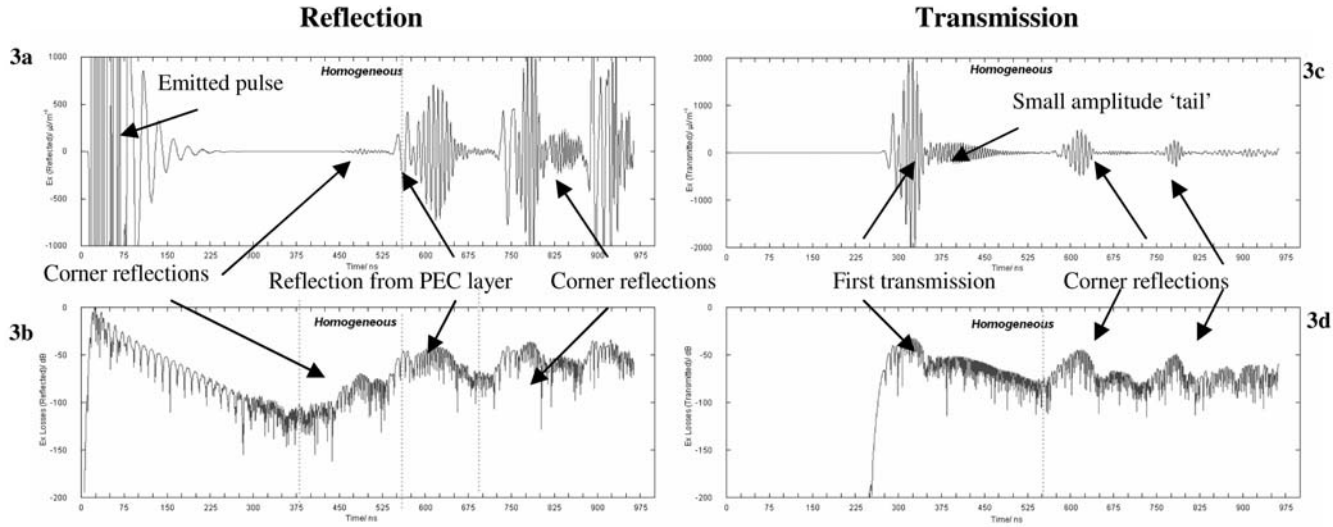

Figs. 3–9. The 90 MHz radar simulations for propagation through the dielectric models (see Table 1), showing the amplitude of the *Ex* component in μVm^{-1} of the reflected (a) and transmitted (c) signals, and normalized reflected (b) and transmitted (d) losses in dB with time. Homogeneous (above), porous homogeneous (Fig. 4), layered (Fig. 5), 20 volume percent 5 m (Fig. 6) and 15 m (Fig. 7) radius inclusions, and 40 volume percent 5 m radius inclusions of porous (Fig. 8), and rocky (Fig. 9) compositions.

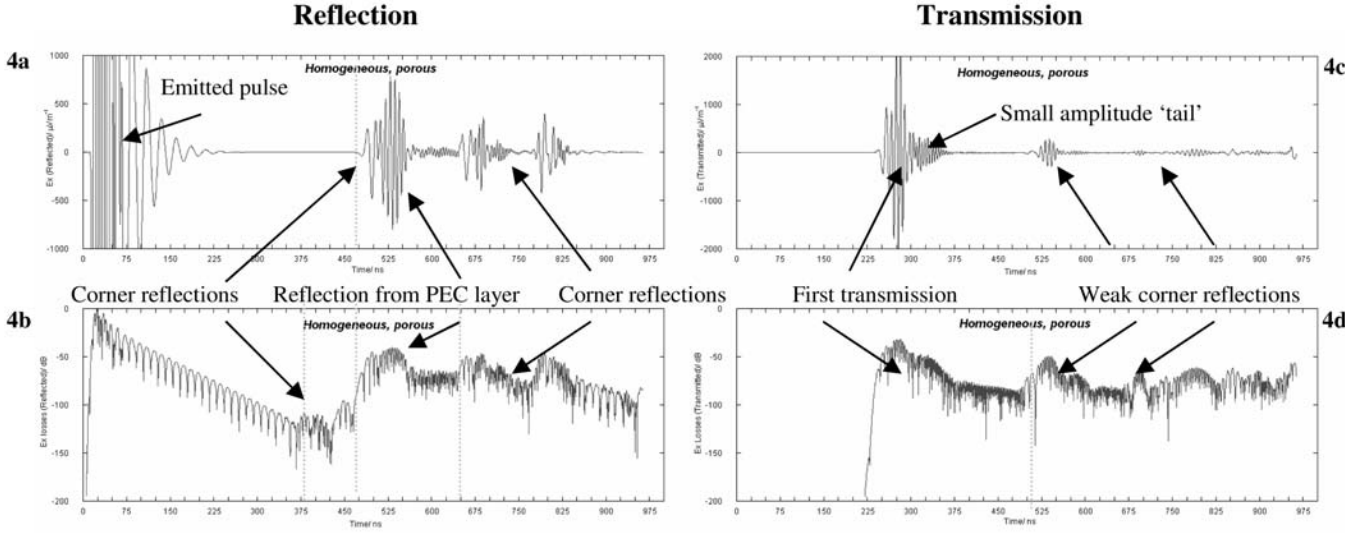

Fig. 4.

broadening is obvious in the transmitted radar signal for the homogeneous and layered models. In these models, the main transmitted signal length of about 60 ns for the porous homogeneous model (Fig. 4c) broadens to about 75 ns and 150 ns in the homogeneous and layered models, respectively (Figs. 3c and 5c). The increased broadening in the layered model occurs as a result of the higher relative permittivity and hence slower propagation velocity. The transmitted pulse is also lengthened by reflections from the dust layer which form a small amplitude "tail" to the main transmitted pulse in the homogeneous models (Figs. 3c and 4c).

The amplitude of the reflected signals in each of these models is determined by the dielectric contrast between the materials at the reflecting interface. A lower dielectric constant, as in the porous homogenous model, presents less dielectric contrast with the free space surrounding the model geometry, resulting in reduced clutter effects from reflections from the corners, and in this geometry, an increased amplitude reflection (compared to the homogeneous model) of about 700 μVm^{-1} (at 525 ns) from the PEC base layer (Fig. 4a). For the layered model, the reflected signal (Fig. 5a) clearly shows reflections from the base of each layer, with the first layer at 225 ns, the second layer at 425 ns, and the third layer (the PEC interface) reflection combined with the corner reflections at about 600 ns. The "peaks" on the normalized loss curve also identify these layers (labeled in Fig. 5b). In transmission, the corner reflections observed at 550 ns and 750 ns in the homogeneous model (Fig. 3c) are indistinguishable in the models with layers or inclusions (Figs. 5c and 6c).

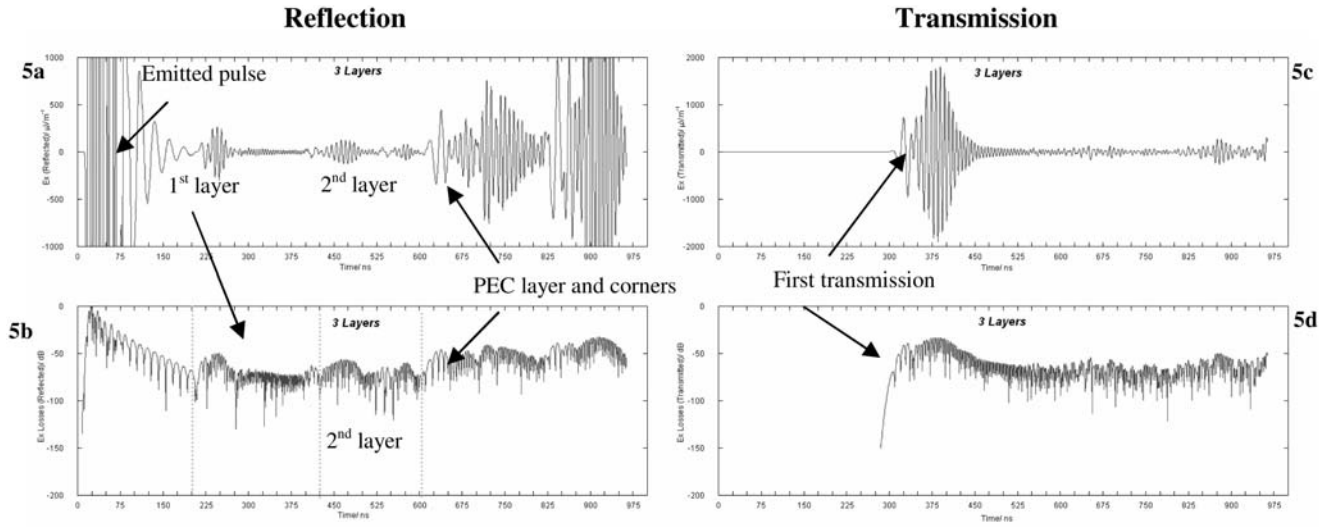

Fig. 5.

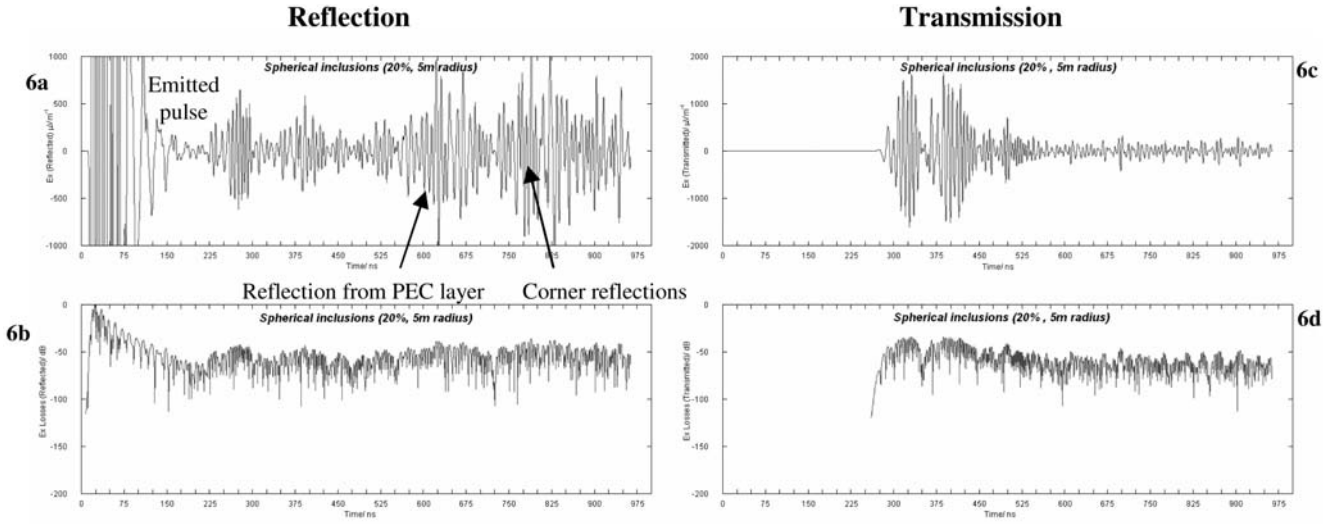

Fig. 6.

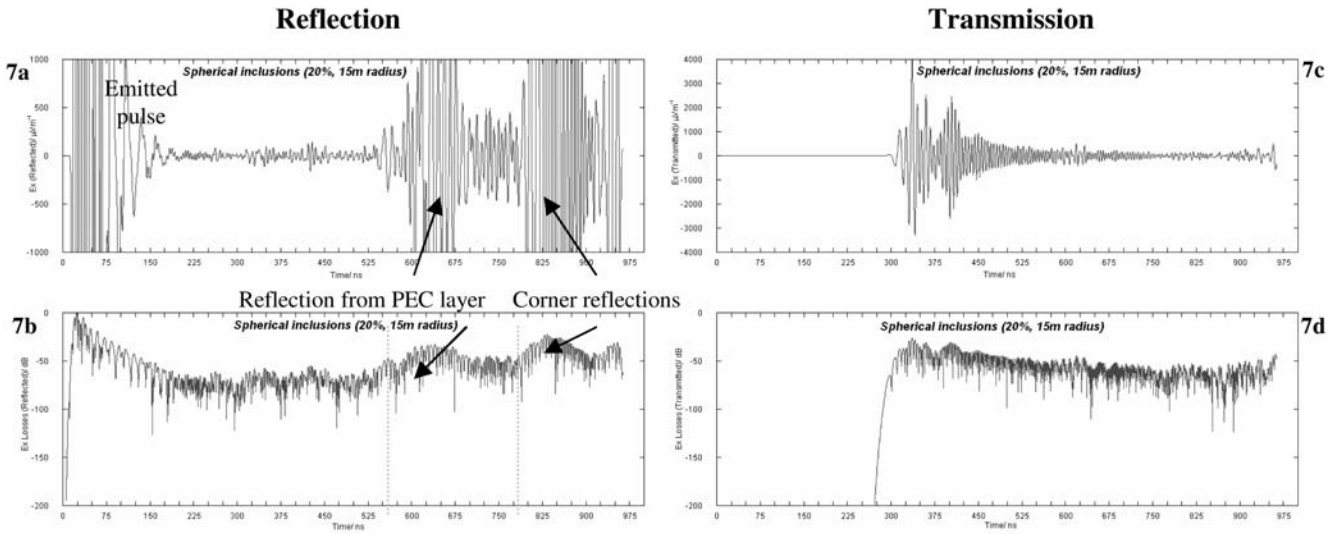

Fig. 7.

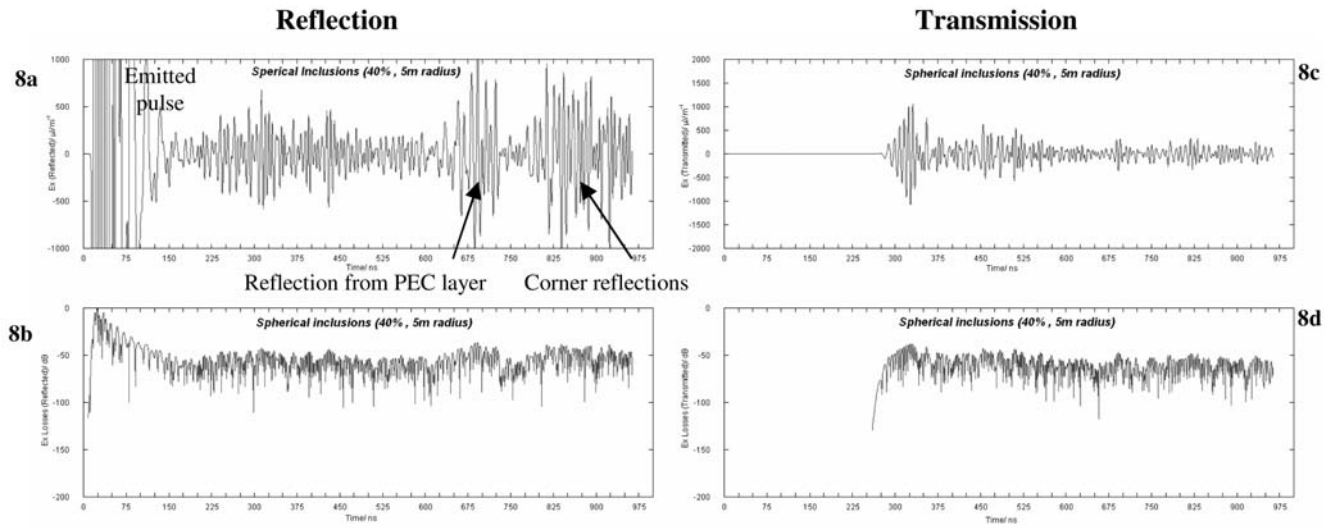

Fig. 8.

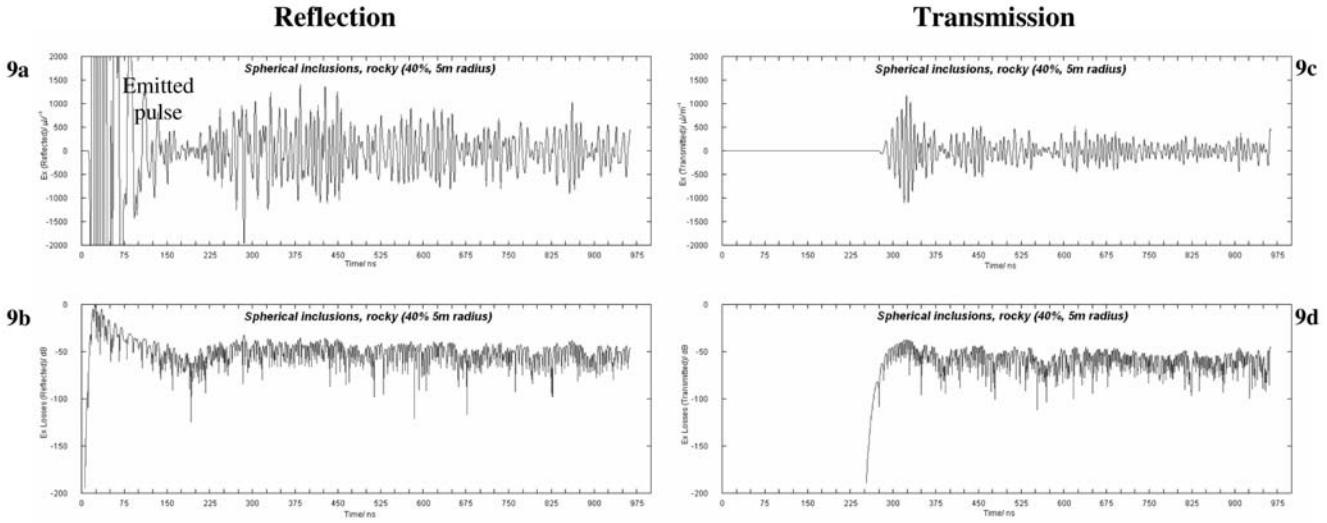

Fig. 9.

The reflected signal from the model with 20 volume percent 5 m inclusions (Fig. 6a) shows a continuously high amplitude (>250 μVm^{-1}) signal and relatively constant normalized loss value (Fig. 6b). This results from multiple reflections from the inclusions, with superposed reflections from the PEC layer at around 600 ns and from the corners at around 750 ns. Reflections from inclusions rapidly distort the radar signal, as observed in the time sequence slides of Fig. 2c. These reflections also cause depolarization of the initial waveform resulting in the similar magnitude of the *Ex* and *Ey* components of the transmitted and reflected signals.

The Effect of Inclusions

As already described, the presence of inclusions provides interfaces for reflection and scattering. Consequently, the *Ey* component of the transmitted and reflected signals for models with inclusions are large and comparable in magnitude to the *Ex* component.

Increasing the size of the inclusions from 5 m to 15 m radius causes a decrease in the average amplitude of the reflected radar waves from about 200 μVm^{-1} for the models with 5 m radius inclusions (Figs. 6a and 8a) to less than 100 μVm^{-1} for the model with 15 m radius inclusions (Fig. 7a). This is due to the decrease in the number of interfaces within a certain volume. Comet models with inclusions significantly larger than the wavelength of propagation (~2.5 m) thus present a more homogeneous structure, with radar signals similar to those through the homogeneous comet nucleus models (compare Figs. 3a and 4a–7a). However, the inclusions do provide interfaces for reflection so the transmitted and reflected *Ey* signals for the model with 15 m radius inclusions are still comparable in magnitude to the *Ex* components, unlike the

homogeneous models, and the normalized loss curve in reflection (Fig. 7b) shows a briefer period of exponential decay than for the homogeneous models (Figs. 3b and 4b).

If the number of inclusions per unit volume is increased, there are more interfaces for reflection, increasing the clutter of the reflected signal (compare Figs. 6a and 8a), and causing de-polarization of the radar wave, thus decreasing the magnitude of the *Ex* component of the transmitted signal from an average of 500 μVm^{-1} in Fig. 6c to 250 μVm^{-1} in Fig. 8c.

An increase in the dielectric contrast between the inclusions and the background icy matrix in these models resulted in an increase in the average reflected signal from about 300 μVm^{-1} with the porous "dirty ice" inclusions (Fig. 8a) to about 500 μVm^{-1} with the porous rocky inclusions (Fig. 9a). However, this increase in amplitude may not be immediately distinguished from the increased clutter of the reflected signal resulting from multiple reflections due to an increase in the volume percent of inclusions (as in Figs. 6a and 8a).

CONCLUSIONS AND PERSPECTIVE

Simulation of the propagation of radar waves through different dielectric comet nuclei models has shown that it is possible for a radar sounding experiment like CONSERT to distinguish structural variation in the comet nucleus by performing temporal analysis of the amplitude and losses of the reflected and transmitted radar signals.

Although this study was only carried out for sections of a model comet, it is clear that radar propagating through a body with different structural elements such as layers or inclusions will present significantly distinguishable transmitted and reflected signals. From the electromagnetic characterization of sections of comet nuclei representing the theoretical state of knowledge of comet nuclei structure, our study shows that interpretation of the internal structure is feasible. The distinguishing features for each model are summarized below.

Homogeneous Nucleus

In reflection mode, a homogeneous nucleus is identifiable by the lack of reflected waves from any internal structures and by the exponential decrease of the radar losses after transmission. A very porous nucleus will present less of a dielectric contrast to the surrounding space so will have a relatively low amplitude reflected signal. To identify reflections from a surface dust layer, the layer would have to be >10 m thick to avoid loss of the signal to the received emitted pulse. The broadening of the waveform in transmission would also be related to the relative permittivity (determined by porosity and composition) of the comet nucleus. As reflections from a homogeneous nucleus are limited, the *Ey* component of the radar signal would be much smaller than the *Ex* component.

Layered Nucleus

The presence of layers larger than the radar wavelength could be detected from reflected radar signals, but could be difficult to infer from the transmitted signal only. Thin, irregular layers representing inhomogenities within the comet nucleus would result in more reflection, scattering and depolarization of the radar signal, similar to that produced by small inclusions.

Nucleus with Inclusions

Inclusions in the comet nucleus cause reflections that result in a distorted waveform, and *Ey* component comparable in magnitude to the *Ex* component of the electric field which imply that the signal is substantially depolarized. Inclusions significantly larger than the wavelength of propagation result in fewer reflections within the bulk of the nucleus, presenting a more homogeneous structure. This investigation has shown that large amplitude transmitted and reflected signals could indicate the presence of several small inclusions, or fewer rocky inclusions in a background icy matrix. This ambiguity could be resolved by constraints on the density and porosity for the comet inferred from non-gravitational effects on the motion of the comet nucleus.

In these simulations it was very difficult to completely avoid the "clutter" of reflections from the corners of the models, but these could be identified from the simulation time sequence slides that showed the progression of the wave inside the models for a given time step. Radar investigations of comet 67P/C-G may also be subject to clutter from reflections from topographic features at the surface of the comet that may increase data complexity in the radar returns. The orbiting Rosetta spacecraft will be able to provide some information on the surface topography of the comet nucleus to aid the interpretation of the returned radar data.

The validity of the dielectric models presented in this simulation relies on the accuracy of the present day knowledge of comet structure and composition. The in-situ measurements to be carried out by the Rosetta lander will be able to offer improved estimates of the surface composition useful for radar data interpretation. A seven-year wait must be endured until CONSERT returns its radar data. During this time, more experiments and simulations will be carried out to increase the capability of understanding the dielectric and scattering losses in the cometary nucleus, which will significantly improve the CONSERT data inversion, as well as prepare for similar sounding experiments for near-Earth objects.

Acknowledgments–The authors would like to thank Dr. Kevin Righter from NASA Johnson Space Center and Drs Wlodek Kofman and Alain Hérique from Laboratoire de Planetologie de Grenoble for helpful discussions, and the two anonymous

reviewers for their suggestions. R. A. Carley would also like to thank Dr. Bill Proud of the Fracture Group, Cavendish Laboratory, Cambridge, and Professor Kathy Whaler of the School of Geosciences, The University of Edinburgh. This work is funded under NASA Planetary Geology and Geophysics program by the grant PGG04-000-0059 and LPI Cooperative Agreement NCC5-679. This paper is a Lunar and Planetary Institute Publication no. 1340.

Editorial Handling—Dr. Louise Prockter

REFERENCES

Asphaug E. and Benz W. 1994. Density of comet Shoemaker-Levy-9 deduced by modelling breakup of the parent rubble pile. *Nature* 370:120–124.

Barbin Y., Kofman W., Nielsen E., Hagfors T., Seu R., Picardi G., and Svedhem H. 1999. The CONSERT instrument for the Rosetta mission. *Advances in Space Research* 24:1115–1126.

Barriot J. P., Kofman W., Hérique A., Leblanc S., and Portal A. 1999. A two dimensional simulation of the CONSERT experiment (Radio tomography of comet Wirtanen). *Advances in Space Research* 24:1127–1138.

Belton M. J. S., Thomas P., Veverka J., Schultz P., A'Hearn M. F., Feaga L., Farnham T., Groussin O., Li J.-Y., Lisse C., McFadden L., Sunshine J., Meech K. J., Delamere W. A., and Kissel J. 2007. The internal structure of Jupiter family cometary nuclei from Deep Impact observations: The "talps" or "layered pile" model. Icarus 191:573–585.

Benna M., Piot A., Barriot J.-P., and Kofman W. 2002. 2-D data set generation and inversion simulation of radio waves propagating through a two-dimensional comet nucleus (CONSERT experiment). *Radio Science* 37:1092–1107.

Brownlee D. E., Hörz F., Newburn R. L., Zolensky M., Duxbury T. C., Sandford S., Sekanina Z., Tsou P., Hanner M. S., Clark B. C., Green S. F., and Kissel J. 2004. Surface of young Jupiter family comet 81P/Wild 2: View from the Stardust spacecraft. *Science* 304:1764–1769.

Carley R. A. and Heggy E. 2006. Characterization of the density-dependent dielectric properties of Mars-like soils: Implications for Mars radar studies (abstract #1261). 37th Lunar and Planetary Science Conference. CD-ROM.

Davidsson J. R. and Gutiérrez P. J. 2005. Nucleus properties of comet 67P/Churyumovv-Gerasimenko estimated from non-gravitational force modelling. *Icarus* 176:453–477.

Donn B. D. 1990. Formation and structure of fluffy cometary nuclei from random accumulation of grains. *Astronomy and Astrophysics* 235:441–446.

Farinella P. and Davis D. R. 1996. Short-period comets: Primordial bodies or collisional fragments? *Science* 273:938–941.

Goldstein R. M., Jurgens R. F., and Sekanina Z. 1984. A radar study of comet IRAS-Araki-Alcock 1983d. *The Astronomical Journal* 89:1745–1754.

Gombosi T. I. and Houpis H. L. F. 1986. An icy-glue model of cometary nuclei. *Nature* 324:43–44.

Harker D. E., Wooden D. H., Woodward C. E., and Lisse C. M. 2002. Grain properties of comet C/1995 O1 (Hale-Bopp). *The Astrophysical Journal* 580:579–597.

Heggy E., Carley R. A., Kofman W., Clifford S. M., Hérique A., Williams I. P., Levasseur-Regourd A.-C. 2006a. Dielectric properties of dirty-ice and FDTD simulation of radar propagation through comet nuclei geoelectrical models to support radar-probing investigation of the comet 67P/Churyumov-Gerasimenko. Workshop on Spacecraft Reconnaissance of Asteroid and Comet Interiors. LPI Contribution 1325. pp. 47–48.

Heggy E., Carley R. A., Pommerol A., Clifford S. M., and Morris R. V. 2006b. Density, temperature, and frequency dependent model of the dielectric map of the Martian surface (abstract #2140). 37th Lunar and Planetary Science Conference. CD-ROM.

Heggy E., Asphaug E., Carley R. A., Safaeinili A., and Righter K. 2007. Dielectric properties of chondrites and their implication in radar sounding of asteroid interiors (abstract #1596). 38th Lunar and Planetary Science Conference. CD-ROM.

Hérique A., Kofman W., Hagfors T., Caudal G., and Ayanides J.-P. 1999. A characterization of a comet nucleus interior: Inversion of simulated radio frequency data. *Planetary and Space Science* 47: 885–904.

Kofman W., Barbin Y., Klinger J., Levasseur-Regourd A.-C., Barriot J. P., Hérique A., Hagfors T., Nielsen E., Grün E., Edenhofer P., Kochan H., Picardi G., Seu R., van Zyl J., Elachi C., Melosh J., Veverka J., Weissman P., Svedhem L. H., Hamran S. E., and Williams I. P. 1998. Comet nucleus sounding experiment by radiowave transmission. *Advances in Space Research* 21:1589–1598.

Kunz K. and Luebbers R. J. 1993. *The finite difference time domain method for electromagnetics*. Boca Raton, Florida: CRC Press. 464 p.

Lamy P. L., Toth I., Jorda, L., Weaver H. A., and A'Hearn M. 1998. The nucleus and inner coma of comet 46P/Wirtanen. *Astronomy and Astrophysics* 335:L25–L29.

Langevin Y., Kissel J., Bertaux J. L., and Chassefiere E. 1987. First statistical analysis of 5000 mass spectra of cometary grains obtained by PUMA 1 (Vega 1) and PIA (Giotto) impact ionization mass spectrometers in the compressed modes. *Astronomy and Astrophysics* 187:761–766.

Parkhomenko E. I. 1967. *Electrical properties of rocks*. New York: Plenum Press. 314 p.

Petrenko V. F. and Whitworth R. W. 1999. *Physics of ice*. Oxford: Oxford University Press. 373 p.

Prialnik D.1998. Modelling gas and dust release from comet Hale-Bopp. *Earth, Moon and Planets* 77:223–230.

Prialnik D., Benkhoff J., and Podolak M. 2004. Modelling the structure and activity of comet nuclei. In *Comets II*, edited by Festou M. C., Keller H. U., and Weaver H. A. Tucson, Arizona: The University of Arizona Press. pp. 359–388.

Rickman H. 1993. Cometary nuclei. In *Asteroids comets meteors 1993*, edited by Milani A., Di Martino M., and Cellino A. Dordrecht: Kluwer Academic Publishers. pp. 297–312.

Scotti J. V. and Melosh H. J. 1993. Estimate of the size of comet Shoemaker-Levy 9 from a tidal breakup model. *Nature* 365:733–735.

Sykes M. V. and Walker R. G. 1992. Cometary dust trails. I—Survey. *Icarus* 95:180–210.

Weissman P. R. 1986. Are cometary nuclei primordial rubble piles? *Nature* 320:242–244.

Weissman P. R., Asphaug E., and Lowry S. C. 2004. Structure and density of cometary nuclei. In *Comets II*, edited by Festou M. C., Keller H. U., and Weaver H. A. Tucson, Arizona: The University of Arizona Press. pp. 337–357.

Whipple F. L. 1950. A comet model. I. The acceleration of comet Encke. *The Astrophysical Journal* 111:375–394.

Yee K. S. 1966. Numerical solution of initial boundary value problems involving Maxwell's equations in isotropic media. *IEEE Transactions on Antennas and Propagation* 14:302–307.